

DYNAMIC CONTROL ASPECTS OF THE SHIPBOARD LAUNCH OF UNMANNED AIR VEHICLES

Crump, M.R. , Riseborough, P. , Bil, C. , Hill, R.

Sir Lawrence Wackett Centre for Aerospace Design Technology, R.M.I.T. University, Australia.

Keywords: UAV, control, launch, ship, aircraft, LQG

Abstract

Fully autonomous control of the launch of UAV's from on board a ship is a problem in the UAV control field. Current solutions are to remotely pilot the UAV until a safe operating trajectory is reached and to limit the launch window to a restricted set of conditions. It is desired to launch the UAV autonomously under a wide set of conditions, and as such a robust automatic controller is necessary.

This paper will address the suitability of LQG/LTR optimal control theories to the UAV shipboard launch problem. A UAV launch with one of these 'conventional' linear controllers is possible, however it is not the optimal solution and does not provide the degree of robustness necessary for launch in more extreme conditions. The use of this controller is simulated and launch is seen to be possible under less extreme conditions.

1 Introduction

Recent interest in the use of fixed wing Unmanned Air Vehicles (UAVs) for civilian and military surveillance and monitoring has highlighted the need for a method of launching these vehicles from various unconventional locations such as ships. Normal launch techniques using a runway may not be applicable to these situations so other methods are necessary. These methods include techniques such as ramp launching and rocket-assisted launching.

In the past, it has been quite common for the

UAV to be remotely piloted during the launch phase, switching to fully autonomous mode after the UAV has cleared the area of ship influence and all transients from the launch have dissipated. It is desirable to have fully autonomous control of the UAV for the entire mission, even going as far as autonomous launch decisions (the UAV will decide when to launch itself). However, when designing a controller to guide the UAV through the launch process, several problems arise which make control design relatively complicated. Some of these problems include ship motion effects, irregular atmospheric and turbulence effects caused by the ship's superstructure and waves, the rapid acceleration of the aircraft and the non-linear dynamics present in low speed high angle of attack flight. Any controller used should thus have some degree of robustness.

The Linear Quadratic Gaussian (LQG) control theory and corresponding Loop Transfer Recovery (LTR) control theory have been successfully applied to aircraft control in the past [14] and have become a baseline for modern control theories. This theory will be applied to the ship launch case.

2 Dynamic Models

2.1 Aircraft Model

2.1.1 Fully nonlinear dynamic model

A fully nonlinear dynamic model of a 6 degree of freedom (DOF) fixed wing aircraft is used. This model is generated from a combination of

theoretical analysis, wind tunnel data and manufacturer specifications. The actual model used within the simulation is an adaption of the UAV Ariel developed by the University of Sydney [9]. This UAV is shown in figure 1. It has a wingspan of 3m and carries a 12 kg payload giving a maximum take-off weight of 32kg.



Fig. 1 Ariel UAV [9]

The nonlinear model has been developed in the standard general state space formulation given by equation 1.

$$\begin{aligned} \dot{\mathbf{v}}_B &= \frac{\mathbf{F}_B}{m} - \boldsymbol{\omega}_B \times \mathbf{v}_B + B_B \mathbf{g}_0 \\ \dot{\boldsymbol{\omega}}_B &= -J^{-1}(\boldsymbol{\omega}_B \times (J\boldsymbol{\omega}_B)) + J^{-1}\mathbf{T}_B \\ \dot{\boldsymbol{\Phi}} &= \boldsymbol{\xi}(\boldsymbol{\Phi})\boldsymbol{\omega}_B \\ \dot{\mathbf{p}}_{NED} &= B_B^T \mathbf{v}_B \end{aligned} \quad (1)$$

where:

- \mathbf{v}_B = aircraft velocity vector
- $\boldsymbol{\omega}_B$ = aircraft angular velocity vector
- $\boldsymbol{\Phi}$ = aircraft Euler angles
- \mathbf{p}_{NED} = aircraft navigation vector
- \mathbf{F}_B = aircraft force vector
- \mathbf{T}_B = aircraft torque vector
- \mathbf{g}_0 = gravity vector
- J = aircraft inertia matrix
- m = aircraft mass
- $\boldsymbol{\xi}$ = aircraft attitude transformation
- B_B = inertial top body transformation

These equations are implemented in the Matlab Simulink environment. Details of this implementation can be found in [3].

2.1.2 Linearised dynamic model

The nonlinear model described in section 2.1.1 is linearised about certain trimmed operating conditions. This process is accomplished by perturbing the state and control variables from the steady state conditions to calculate the Jacobian matrices for the linear state space formulation given in equation 2. Further details about this procedure can be found in [13].

$$\begin{aligned} \dot{x} &= Ax + Bu \\ y &= Cx + Du \end{aligned} \quad (2)$$

where A,B,C,D are aircraft state space matrices describing the open loop dynamic response and:

- x = state variables
- u = control inputs
- y = output variables

These linear models are then used for the controller design.

2.2 Ship Model

Certain variables play an important role in the modeling of ship motion. One of the most important of these is the sea state. The sea state describes the severity of the ocean motion. More detail can be found in [10] and [11]. Sea state 6 has been used as a worst case scenario for launching a UAV from a ship, with sea states higher than this considered too rough for safe launching. Sea state 6 corresponds to very rough seas with a significant wave height up to 6 meters.

The main ship model is based upon the premise of simple harmonic motion. Generic data for a frigate sized naval vessel as shown in figure 2 was used to supply approximate motion frequencies and amplitudes [6]. These frequencies and amplitudes correspond to a RMS value as described in [11]. The worst case motion used corresponds to the average value of the top $\frac{1}{10}$ of

motion amplitudes, which is given as 2.55 times the RMS value.

Using these worst case values, harmonic motion can be generated for each of the six degrees of freedom of the ship. Each DOF is considered uncoupled with respect to any other.

Another important factor when considering the aircraft/ship interface is the position of the UAV aboard the ship. Obviously, if the UAV is located away from the center of motion, significant translations may occur due to the rotation of the ship.



Fig. 2 Frigate class naval vessel

2.3 Launcher Model

The aircraft is to be launched using a catapult technique along an inclined ramp. This ramp will constrain the aircraft to move in only the forwards dimension. This prevents the aircraft from experiencing any unwanted rotations or translations during launch.

The launcher has been modeled as applying a constant force to the aircraft until it has left the ramp. The force is calculated using basic dynamic relationships between the length of the ramp, the desired acceleration and the required airspeed. This velocity should typically be about 1.5 times the stall velocity of the aircraft.

As we are dealing with relatively small lightweight aircraft which have not been de-

signed for large structural loads, the acceleration which can be applied to the aircraft is limited (as compared to missiles which are designed for very large structural loads).

2.4 Turbulence, Gust and Wind model

There has been little work published upon the influence of a ship's structure upon its airwake [5]. The standard turbulence model used within aircraft simulations is the Von Karman model (or its simplified counterpart, the Dryden model) [1]. These models pass white noise through a filter designed from a specific turbulence spectrum. The model contained in [1] also allows for aircraft carrier airwake interference. This contribution has been used, although it is noted that the airwake behind an aircraft carrier will be significantly different to that behind a frigate.

As these processes involve random numbers, a worst case scenario will only be generated very rarely. In controller testing, it is desired to test the controller through worst case conditions. As such, the simulation allows direct input of gust velocities to the aircraft during the launch process.

There is also a steady state wind model which allows for varying strength winds from all directions.

3 Control Technique

3.1 Control Objectives

It is unlikely that the controller that directs the UAV throughout the mission will be adequate to guide the aircraft successfully through the ship launch process. A separate launch controller is therefore necessary. This controller will launch the aircraft from the ship and then once the aircraft has reached a safe operating regime, will switch to the mission controller. This requires an endpoint for the launch controller.

This endpoint should be selected to allow optimal trajectory control throughout the mission. The endpoint should be far enough into the flight so the aircraft has climbed safely away from the

ship to a reasonable height, but not too far into the flight as to compromise the mission.

Once the endpoint is selected, the necessary trajectory must be determined. Again, a compromise is necessary. It is desirable for the aircraft to climb as rapidly as possible, to minimise the risk of collision with either the ship or the ocean. However, to achieve maximum rate of climb with low velocities requires high angles of attack. At these high angles of attack, in the turbulent environment behind the ship, aircraft stall is highly probable. At these low altitudes, this stall may be catastrophic. Thus, a rate of climb less than the maximum rate of climb is suggested.

For the case of the UAV Ariel, a launch speed of 30 m/s is chosen and a corresponding climb angle of 12°. The stall speed of the Ariel is approximately 20 m/s and the maximum rate of climb is approximately 18°.

The other important consideration is what needs to be controlled. In this situation, we require good climb performance, so the main emphasis on control is on holding a certain climb angle. Other control objectives applied include velocity hold, and laterally, a bank angle/turn coordinator is used to maintain 'straight' flight. (note that this can easily be changed to perform a heading hold function)

3.2 LQG/LTR Controller Design

The standard Linear Quadratic Gaussian (LQG) control design methodology with Loop Transfer Recovery (LTR) has been used to design a suitable launch controller.

Full details of these methods can be found in [8, 12, 13, 7, 2].

Given a state space plant model in the form

$$\dot{x} = Ax + Bu + \Gamma w \quad (3)$$

$$y = Cx + v \quad (4)$$

where Γ corresponds to a noise weighting matrix and w and v are uncorrelated white noise with covariances given by

$$E\{ww^T\} = W \geq 0 \quad E\{vv^T\} = V > 0 \quad (5)$$

the standard LQG design principle requires the feedback control law which minimises the cost

$$J = \lim_{T \rightarrow \infty} E \left\{ \int_0^T (z^T Q z + u^T R u) dt \right\} \quad (6)$$

where $z = Mx$ is some combination of the states and $Q = Q^T$ and $R = R^T$ are weighting matrices. The LQG method is solved by generating an optimal state estimate using a Kalman filter which then drives the optimal state regulator given by the linear quadratic regulator problem (LQR). This procedure reduces the problem to two sub problems, both of which can be solved relatively easily. The structure of this compensator is shown in figure 3.

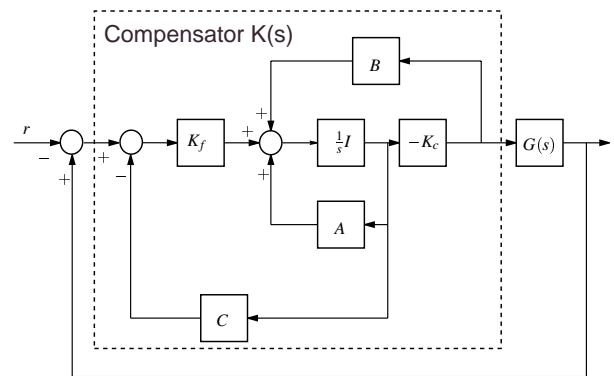


Fig. 3 LQG compensator structure

The optimal state feedback matrix is given by

$$K_c = R^{-1} B^T P_c \quad (7)$$

where P_c is the positive semi-definite solution to the algebraic Riccati equation

$$A^T P_c + P_c A - P_c B R^{-1} B^T P_c + M^T Q M = 0 \quad (8)$$

and likewise, the Kalman filter gain matrix is given by

$$K_f = P_f C^T V^{-1} \quad (9)$$

where P_f is the positive semi-definite solution to the algebraic Riccati equation

$$P_f A^T + A P_f - P_f C^T V^{-1} C P_f + \Gamma W \Gamma^T = 0 \quad (10)$$

These equations can be solved easily using any one of a number of mathematical packages.

This procedure will generate stable controllers for arbitrary choice of Q and R , however, these controllers may have poor stability and performance robustness. The Loop Transfer Recovery procedure has been developed to allow good recovery of the full state feedback properties [4].

The LTR procedure can be conducted in two ways. The first way involves designing a suitable quadratic regulator by manipulating the Q and R matrices. The Kalman filter is then synthesized by setting $\Gamma = B$, $W = I$ and $V = \rho I$. The value of ρ can be decreased causing the return ratio at the input of the compensated plant to approach that of $-K_c(j\omega I - A)^{-1}B$ until a satisfactory frequency range of recovery has occurred. The dual of this procedure involves the design of a Kalman filter by manipulation of the matrices W and V until an open loop return ratio $-G(s)K(s)$ that would be satisfactory at the plant output is achieved. The optimal state feedback regulator is then synthesized by setting $M = C$, $Q = I$ and $R = \rho I$ and reducing ρ until satisfactory recovery occurs.

This dual procedure has been used in this case as it is more appropriate for design for performance.

3.3 Shaping of the controlled system

The performance of a system can be represented by the sensitivity function S and the complementary sensitivity T , given by

$$S(s) = \frac{I}{I + G(s)K(s)} \quad (11)$$

$$T(s) = \frac{G(s)K(s)}{I + G(s)K(s)} = I - S \quad (12)$$

where $G(s)$ is the plant and $K(s)$ is a specified controller. Given these two functions, our system can be re-written as

$$y(s) = S(s)d(s) + T(s)r(s) - T(s)m(s) \quad (13)$$

where y is the system output, d represents any external disturbances, r is a reference command

and m corresponds to any sensor noise. Obviously, we wish our output to track our reference command perfectly. Thus, according to equations 12 and 13 we have conflicting objectives. To minimise the effects of disturbances and sensor noise, we require both T and S to be small, but given that $T + S = I$, this is not possible. The usual solution is to minimise each over a range of frequencies (usually disturbances will be low frequency, whilst measurement noise will be high frequency).

In the single input single output (SISO) case, the values of S and T are unique for each frequency, however when the multiple input multiple output (MIMO) case is considered, several values of S and T will exist at each frequency (as the inputs and outputs will consist of matrices). To get a good representation of the values or size of these matrices, matrix norms are typically used. One of the most commonly used norms is the Hilbert norm or the singular values.

The singular value decomposition of any $l \times m$ matrix G is given by

$$G = U\Sigma V^T \quad (14)$$

where Σ is a $l \times m$ matrix with $\min\{l, m\}$ positive singular values σ_i along the main diagonal in descending order, U is an $l \times l$ matrix of output singular vectors and V is an $m \times m$ matrix of input singular vectors.

The largest gain for any combination of input directions is equal to the maximum singular value, denoted by $\bar{\sigma}(G)$ and the smallest gain for any input direction is equal to the minimum singular value, given by $\underline{\sigma}(G)$. The input and output directions corresponding to these maximum and minimum gains are given by the corresponding columns in the U and V matrices.

Using the singular values of S and T , we can again use the relationships in equation 12. As before, we are interested in keeping S small at low frequencies. The maximum singular value of S , $\bar{\sigma}(S)$ will be the important boundary in this case. Similarly, at high frequencies, to keep T small, the upper boundary will likewise be the maximum singular value of T , $\bar{\sigma}(T)$. By using

the largest singular values, we are effectively assessing the worst case scenario.

4 Design Results

4.1 Controller Design

Two controllers have been developed, the first with no consideration of the surrounding environmental turbulence and the second incorporating robustness to these external disturbances

As stated in section 3.1, the chosen launch condition corresponds to a ramp exit speed of 30 m/s and a corresponding climb angle of 12° . The nonlinear model was linearised about trimmed flight at these conditions. The standard launch position would be at the extreme rear of the ship, facing backwards.

To perform the control design, the linear aircraft model has been decoupled into lateral and longitudinal models. The longitudinal model will control velocity and climb angle, whilst the lateral model will control lateral acceleration and bank angle. Each model has then been scaled and normalised to give approximately equal inputs and outputs (between ± 1). The design for both the longitudinal controller and the lateral controller are performed exactly the same, and as such only the results for the longitudinal design will be presented.

4.1.1 Naive Control Design

The first control design technique takes no account of any external disturbances. The controller design process begins by selecting $\Gamma = B$, $W = I$ and $V = I$. The $\Gamma = B$ choice corresponds to the rejection of control disturbances and should give a controller which performs well in the nominal case. The direct design of the Kalman filter gain gives a return ratio indicated by the blue (dotted) line in figure 4.

As we are concerned with good tracking, the presence of steady state errors is a large concern. Common practice in control theory is to augment the plant with integrators, eliminating the steady state error. Integration requires the addition of poles at the origin. This can lead to mathematical

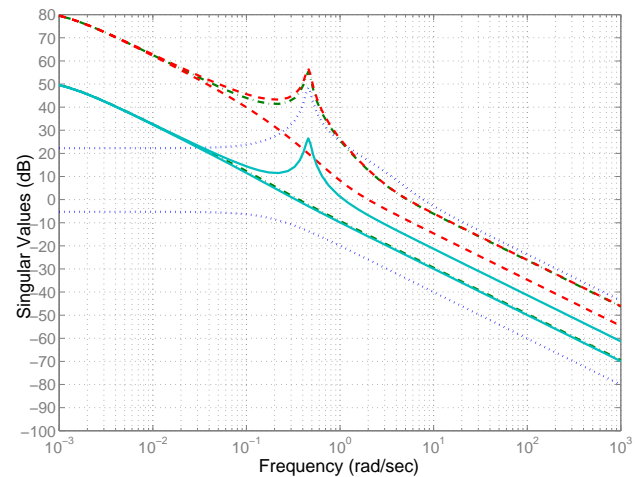


Fig. 4 Longitudinal return ratios for naive controller

problems, and thus the poles are placed slightly into the left half plane. The return ratio of the augmented plant is indicated by the green (dot-dashed) line in figure 4.

The next step is to increase the smallest gain to speed up the elimination of steady state errors. We would like to do this without modifying the maximum gains. This can be achieved by using the singular value decomposition of the return ratio at the desired frequencies. Using the right singular vectors, the weighting matrix W may be modified by scaling this vector. Further details on this procedure can be found in [8]. The return ratios given by this modified procedure are indicated by the red (dashed) line in figure 4.

Whilst in theory, we would like an extremely rapid response, the only practical way to achieve this is by very large and rapid control inputs. As we have physical limits on our controls, such rapid responses are not practical. Thus, to slow the system down somewhat, the weighting matrix may be scaled down appropriately, thus reducing the gains of the entire system and slowing it down. The effects of this are shown by the cyan (solid) line in 4.

This gives an adequate return ratio, and thus the recovery step may begin. Using a recovery value of $\rho = 1E - 12$ gives good recovery up to a frequency of 100 rad/s as shown in figure 5,

where the desired return ratio is shown as the green (dashed) line and the actual recovered return ratio is shown as the blue (solid) line.

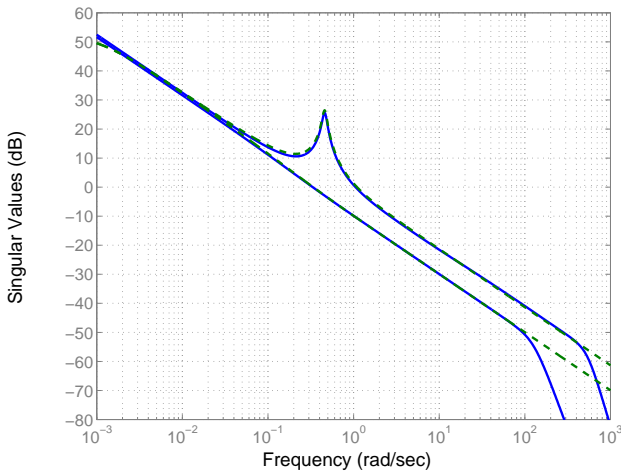


Fig. 5 Longitudinal loop recovery for naive controller

The sensitivity and complementary sensitivity functions given by equations 11 and 12 are shown in figure 6. The sensitivity is shown by the blue (solid) line and the complementary sensitivity is shown by the green (dashed) line. It is easy to see that our goal of minimising the sensitivity at low frequencies has been achieved, and we have also minimised the complementary sensitivity at high frequencies. The local minimum in the sensitivity at approximately 0.5 rad/s corresponds to the oscillatory dynamics of the aircraft at this frequency.

4.1.2 Control Design with respect to gust disturbances

The same procedure as used in the previous section was used to generate a controller that includes robustness to gust effects on the aircraft. In the linearisation procedure mentioned in section 2.1.2, the effects of a three dimensional wind gust input to the aircraft were also linearised. Using these effects, and using the assumption that the gust inputs will be white noise (this assumption may be modified by including some altering dynamics such as a Dryden filter with the gust

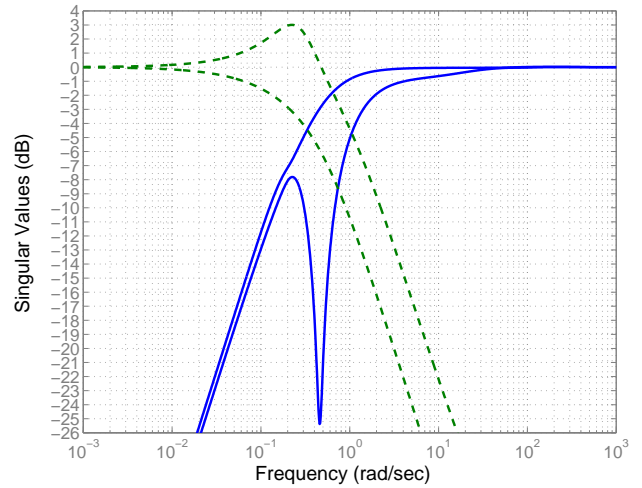


Fig. 6 Longitudinal sensitivity functions for naive controller

dynamics), the control design can be performed again.

In this case, we set Γ as the linearised gust effect matrix (this matrix can be thought of as similar to the control matrix B). The plant is again augmented with integrators and in the same manner as previously, the smallest gain is again balanced with respect to the largest and the entire controller is slowed down to reduce control effort. Figure 7 shows the return ratios for this state estimator. (unaugmented - blue dotted, augmented - green dot dashed, augmented balanced - red dashed and augmented balanced slowed - cyan solid).

Again using a recovery factor of $\rho = 1E - 12$, the recovery again is good as shown in figure 8, however, it is not quite as good as for the naive controller.

The sensitivity functions for this controller are shown in figure 9. These functions are extremely similar to those for the naive controller

5 Simulation Results

The results from several different simulation cases will be presented here. All cases involve the ship traveling north and the standard launch position described in section 3.1. The UAV is launched 10 seconds into the simulation, corre-

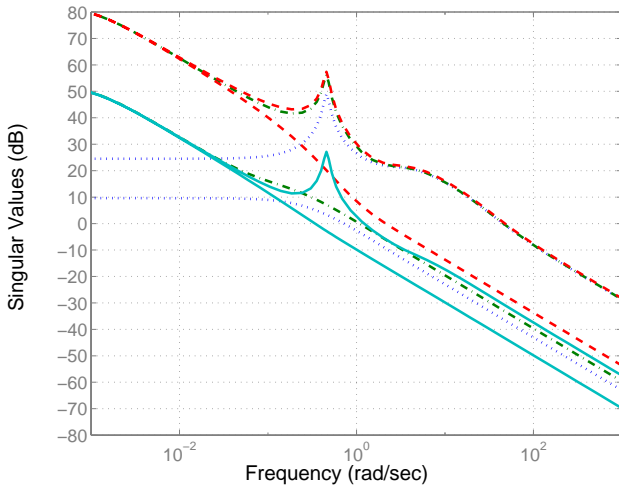


Fig. 7 Longitudinal return ratios for gust disturbance rejection controller

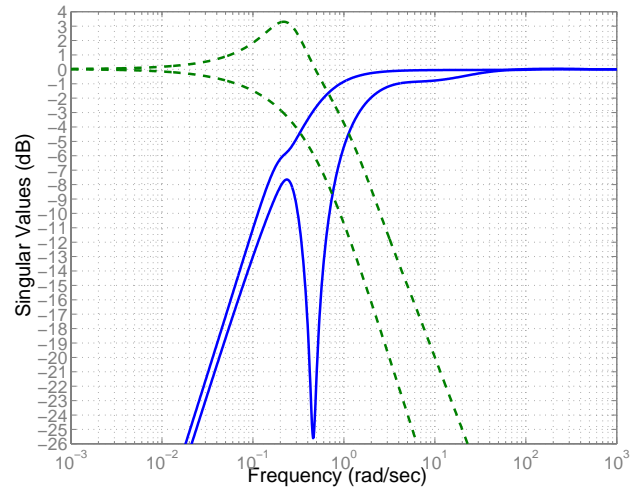


Fig. 9 Longitudinal sensitivity functions for gust disturbance rejection controller

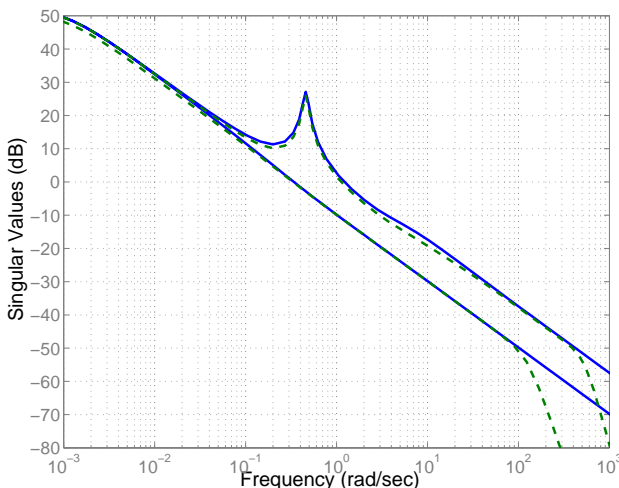


Fig. 8 Longitudinal loop recovery for gust disturbance rejection controller

sponding to a worst case ship position. This corresponds to the ship at maximum pitch (up), maximum heave (down), maximum bank, maximum yaw, maximum surge and maximum sway. These test cases are:

- Case 1. No atmospheric effects, naive controller (blue solid line).
- Case 2. UAV tail wind 10m/s, low turbulence, naive controller (green dotted line).

- Case 3. UAV tail wind 10m/s, low turbulence, gust rejection controller (red dashed line).
- Case 4. UAV worst case side gust square wave amplitude 5 m/s frequency 0.5 Hz , gust rejection controller (cyan dot dashed line).
- Case 5. UAV worst case vertical gust square wave amplitude 5 m/s frequency 0.5 Hz , gust rejection controller (magenta solid line).

The simulation results for the first 30 seconds are shown in figures 10,11,12 and 13. From these figures, it is quite easy to see that case 1 experiences no problems at all, case 2 and 3 both have problems immediately after launch, case 4 has no problems and case 5 causes the UAV to crash. Case 1 illustrates the performance of the naive controller. As can be seen, the aircraft climbs steadily away from the ship, maintaining very little bank angle.

Case 2 and 3 illustrate that in the presence of steady state winds, the gust rejection controller has little effect upon the performance of the aircraft. In both cases, the aircraft experiences a drop after it has left the ramp. This is due to the strong tailwind experienced by the aircraft. It is thought the only way to remedy this situation would be to increase the launch speed.

DYNAMIC CONTROL ASPECTS OF THE SHIPBOARD LAUNCH OF UNMANNED AIR VEHICLES

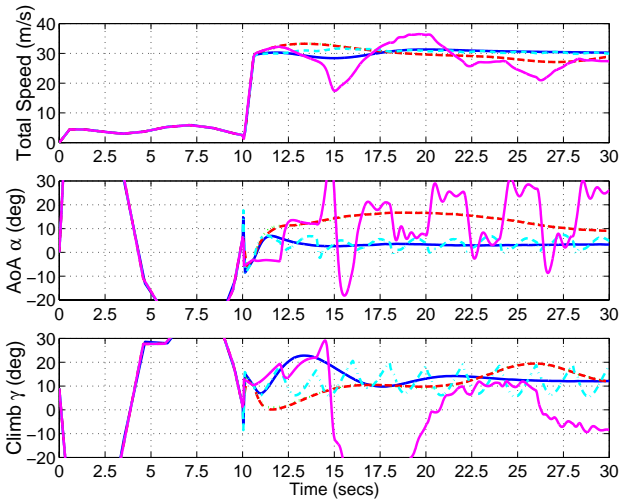


Fig. 10 Simulation results

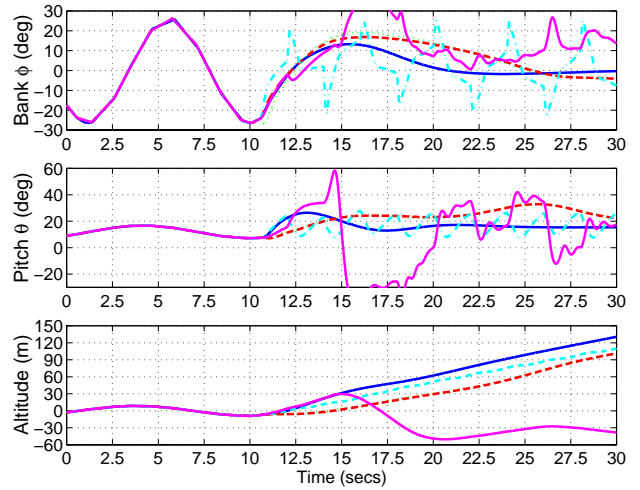


Fig. 12 Simulation results

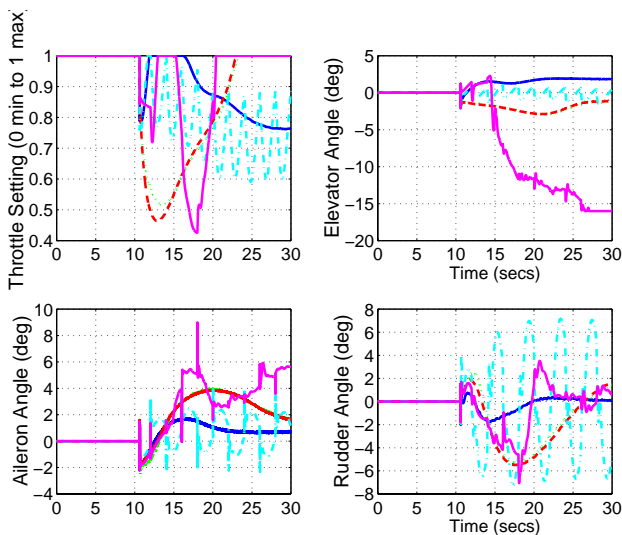


Fig. 11 Simulation results

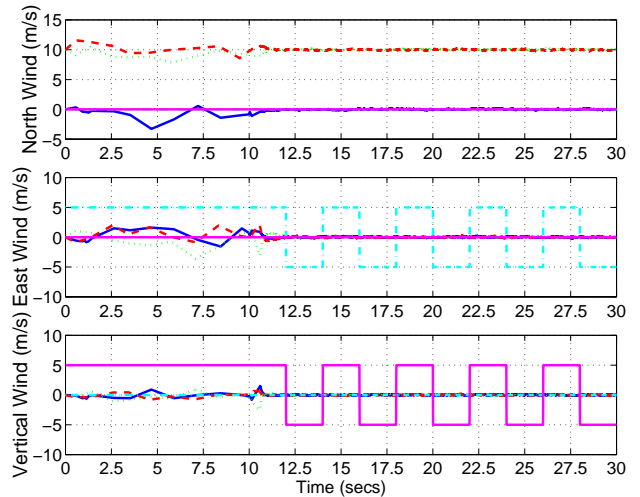


Fig. 13 Simulation results

Case 4 illustrates the benefits obtained from the gust disturbance controller. The aircraft subjected to quite severe crosswind gusts experiences a steady rate of climb with some oscillation in bank angle as would be expected. This oscillation corresponds to the gust frequency used and reaches a peak value of about 30 degrees. For this level of gust, this is deemed satisfactory.

Case 5 illustrates one of the limitations of this controller. A vertical gust of 5m/s causes the aircraft launch to fail. The strong vertical gusts cause aircraft stall which is not recovered.

The stall recovery is hampered by elevator saturation, visible in figure 11. Several options exist to overcome this problem. These include a stall monitoring system and recovery system incorporated within the control system, a controller with a more rapid response time and a controller that has a greater robustness to vertical gusts.

Several other cases also exist where the gust disturbance rejection controller could not adequately control the aircraft through the launch phase.

6 Conclusions

It has been shown through simulation that automatic control of the shipboard launch of UAVs should be possible. A controller has been developed that is capable of rejecting gust disturbances, whilst maintaining good climb performance through the launch phase.

This controller however has been found to be inadequate in situations involving high atmospheric turbulence. Enhancements and other methods of control design are currently in development to enable launch in these situations.

References

- [1] Flying qualities of piloted airplanes. MIL-F-8785C, Military Specification, 5 November 1980. US Department of Defence.
- [2] Anderson B and Moore J. *Linear Optimal Control*. Prentice-Hall, 1972.
- [3] Crump M, Riseborough P, and Bil C. Dynamic simulation of shipboard launch of surveillance type unmanned air vehicles. *Proc IAC 99, Adelaide Australia*, 13th-15th Sep 1999.
- [4] Doyle J and Stein G. Multivariable feedback design: Concepts for a classical/modern synthesis. *IEEE transactions on Automatic Control*, Vol. AC-26, pp 4–16, 1981.
- [5] Healey J. Establishing a database for flight in the wakes of structures. *Journal of Aircraft*, Vol. 29, No 4, pp 559–564, 1992.
- [6] Hope K. Angular motions of an Australian ffg in rough seas ss6-7 - statistics and spectra. Technical Report 96, Australian Defence Force Academy, 1996.
- [7] Kwakernaak H and Sivan R. *Linear Optimal Control Systems*. Wiley, 1972.
- [8] Maciejowski J. *Multivariable Feedback Design*. 1989.
- [9] Newman D and Wong K. Six degree of freedom flight dynamic and performance simulation of a remotely-piloted vehicle. Technical Report Aero.Tech.Note 9301, The University of Sydney, June 1993.
- [10] Rawson K and Tupper E. *Basic Ship Theory Volume 1*. 1983.
- [11] Rawson K and Tupper E. *Basic Ship Theory Volume 2*. 1983.
- [12] Skogestad S and Postlethwaite I. *Multivariable Feedback Control*. 1997.
- [13] Stevens B and Lewis F. *Aircraft Control and Simulation*. 1992.
- [14] Voulgaris P and Valavani L. High performance linear quadratic and h-infinity designs for a supermaneuverable aircraft. *Journal of Guidance, Control and Dynamics*, Vol. 14, No 1, pp 157–165, 1991.